Available online at www.sciencedirect.com
SCIENCE DIRECT®
Journal of Solid State Chemistry 177 (2004) 17–25
JOURNAL OF SOLID STATE CHEMISTRY
http://elsevier.com/locate/jssc

$R_{12}Pt_7In$ (R = Ce, Pr, Nd, Gd, Ho)—new derivatives of the Gd_3Ga_2-type

Ya.V. Galadzhun,[a] V.I. Zaremba,[a,*] Ya.M. Kalychak,[a] V.M. Davydov,[a] A.P. Pikul,[b] A. Stępień-Damm,[b] and D. Kaczorowski[b]

[a] *Inorganic Chemistry Department, Ivan Franko Lviv National University, Kyryla i Mefodiya Str. 6, 79005 Lviv, Ukraine*
[b] *W. Trzebiatowski Institute of Low Temperature and Structure Research, Polish Academy of Sciences, P.O. Box 1410, 50-950 Wroclaw, Poland*

Received 25 February 2003; received in revised form 21 April 2003; accepted 25 April 2003

Abstract

A new compound $Ce_{12}Pt_7In$ was synthesized and its crystal structure at 300 K has been determined from single crystal X-ray data. It is tetragonal, space group $I4/mcm$, $Z = 4$, with the lattice parameters: $a = 12.102(1)$ Å and $c = 14.542(2)$ Å, w$R2 = 0.1102$, 842 F^2 values, 33 variable parameters. The structure of $Ce_{12}Pt_7In$ is a fully ordered ternary derivative of the Gd_3Ga_2-type. Isostructural compounds has been found to form with Pr ($a = 11.976(1)$ Å, $c = 14.478(2)$ Å), Nd ($a = 11.901(1)$ Å, $c = 14.471(2)$ Å), Gd ($a = 11.601(3)$ Å, $c = 14.472(4)$ Å), and Ho ($a = 11.369(1)$ Å, $c = 14.462(2)$ Å). Magnetic properties of $Ce_{12}Pt_7In$, $Pr_{12}Pt_7In$ and $Nd_{12}Pt_7In$ were studied down to 1.7 K. All three ternaries order magnetically at low temperatures with complex spin arrangements. The electrical resistivity of $Ce_{12}Pt_7In$ and $Nd_{12}Pt_7In$ is characteristic of rare-earth intermetallics.

Keywords: Intermetallic rare-earth compounds; Crystal structure; Indium compounds; Magnetic and electrical properties

1. Introduction

The indium compounds with rare earths and platinum were investigated for the first time as far back as 1974 by Ferro and co-workers [1]. Interest to those systems has been renewed in recent years and several articles were published on novel phases: R_2Pt_2In (R = La–Nd, Sm, Gd–Ho) [2,3]; $LaPtIn_4$, $RPtIn_3$ (R = La–Nd, Sm) [3]; RPt_2In_2 (R = La–Nd) [4]; TbPtIn, HoPtIn [5]; PrPtIn, SmPtIn [6]; $Gd_3Pt_4In_{12}$, $Tb_3Pt_4In_{12}$ [7]; $Dy_2Pt_7In_{16}$, $Tb_6Pt_{12}In_{23}$ [8]. A special attention was devoted to cerium compounds due to their remarkable physical properties. To date for the Ce–Pt–In system there was reported the existence of five intermetallics: $CePt_4In$ ($MgCu_4Sn$ structure type) [9], $CePtIn_3$ ($LaRuSn_3$ structure type) [3], CePtIn ($ZrNiAl$ structure type) [10], Ce_2Pt_2In (Mo_2FeB_2 structure type) [2,3] and $CePt_2In_2$ (own structure type) [4]. Among them CePtIn and Ce_2Pt_2In are heavy-fermion paramagnets [11–18], while $Ce_3Pt_4In_{13}$ is a heavy-fermion system that exhibits long-range antiferromagnetic ordering [19].

All the cerium compounds mentioned above form in the region of relatively low concentration of rare earth. In turn our systematic investigation on the Ce–Pt–In phase diagram lead to a discovery of just one ternary phase in the region of high content of cerium, namely $Ce_{12}Pt_7In$. In this article, we report on the constitution, crystal structure and bulk physical properties of this new compound, as well as on its isostructural counterparts $R_{12}Pt_7In$ with R = Pr, Nd, Gd and Ho. Some preliminary account on this work was given in Ref. [20].

2. Experimental

Starting materials for the preparation of $R_{12}Pt_7In$ indides were ingots of rare-earth metals (Johnson Matthey), platinum plate (Degussa) and indium tear drops (Johnson Matthey), all with stated purities greater than 99.9%. In a first step pieces of the rare-earth metal were arc-melted under argon. This procedure strongly reduces a shattering of these elements during the exothermic reactions. Initially Ce–Pt–In alloys with the compositions 6:2:1 and 12:6:1 were synthesized for

*Corresponding author.
E-mail address: vazar@franko.lviv.ua (V.I. Zaremba).

0022-4596/03/$ - see front matter © 2003 Elsevier Inc. All rights reserved.
doi:10.1016/S0022-4596(03)00241-X

the purpose to verify the existence of platinum compounds isostructural to R_6T_2In [21] and $R_{12}T_6In$ [22], where T = Co, Ni. The elemental components were mixed in the ideal 6:2:1 or 12:6:1 atomic ratio and arc melted under argon atmosphere purified over titanium sponge. The samples were remelted twice to ensure good homogeneity. The weight losses after melting were always smaller than 1 wt%. The buttons were subsequently sealed in evacuated silica tubes and annealed at 870 K for 1 month. The samples obtained were stable against air and moisture, as no symptoms of decomposition were observed after several weeks.

Small single crystals for X-ray investigations were isolated by mechanical fragmentation from an annealed button of initial composition $Ce_{0.67}Pt_{0.22}In_{0.11}$. The EDAX analysis with a Philips EDX515-PV9800 scanning electron microscope yielded the composition: Ce—63.0 at%, Pt—32.3 at%, In—4.7 at% being very close to 12:7:1. No impurities were observed in the microprobe spectra. The composition $Ce_{12}Pt_7In$ has subsequently been confirmed by crystal structure refinement from single-crystal X-ray data, that were collected using an automatic four-circle diffractometer KM-4 KUMA DIFFRACTION with graphite monochromatized Mo$K\alpha$ radiation. An analytical absorption correction based on psi-scan data was applied. Hence, for further investigations the alloys $R_{12}Pt_7In$ with R = Ce, Pr, Nd, Gd and Ho were synthesized, as described above. Powder X-ray intensity data were collected at room temperature using an automatic powder diffractometer HZG-4a with Cu$K\alpha$ radiation ($\theta/2\theta$ scan mode, step 0.05°θ, range $2\theta = 15-105°$). Full-profile structural refinements were performed using the program DBWS-9807 [23].

Magnetic properties were studied on polycrystalline samples in the temperature range 1.7–300 K and in applied magnetic field up to 5 T using Quantum Design MPMS-5 SQUID magnetometer. Electrical resistivity measurements were carried out in the temperature interval 4.2–300 K employing conventional four-point DC technique.

3. Results and discussion

3.1. Structure determination

A platelet-like single crystal was first examined by Laue and rotation methods (camera RKV-86, MoK radiation) to establish its symmetry and suitability for X-ray intensity data collection. On the basis of Weissenberg photographs (camera RGNS-2, CuK radiation) a tetragonal symmetry (Laue class $4/mmm$) was established and the lattice parameters were roughly calculated. The initial atomic parameters were deduced from an automatic interpretation of the data obtained by direct methods with SHELXS-97 [24]. The crystal structure was successfully refined applying SHELXL-97 (full-matrix least squares on F^2) [25] using the lattice parameters derived from the powder diffraction data (as being more precise than the single crystal results). The experimental details and some main crystallographic data are listed in Tables 1 and 2. Anisotropic displacement parameters were considered for all the atoms. The occupancy factors were refined in a separate series of least-squares cycles with the purpose to check the correctness of site assignments. The full occupancy within standard deviations was observed for all the sites. The final difference Fourier synthesis revealed no significant residual peaks (see Table 2). The refined atomic parameters are listed in Table 3 and the interatomic distances are given in Table 4. The crystal

Table 1
Lattice parameters of the tetragonal compounds $R_{12}Pt_7In$ (R = Ce, Pr, Nd, Gd, Ho) and some other representatives of the Gd_3Ga_2 structure type[a]

Compound	a (Å)	c (Å)	c/a	V (Å^3)
$Ce_{12}Pt_7In^S$	12.093(2)	14.548(3)	1.2030	2127.5
$Ce_{12}Pt_7In^P$	12.102(1)	14.542(2)	1.2016	2129.8
$Pr_{12}Pt_7In^P$	11.976(1)	14.478(2)	1.2089	2076.5
$Nd_{12}Pt_7In^P$	11.902(1)	14.472(2)	1.2159	2050.1
$Gd_{12}Pt_7In^P$	11.601 (3)	14.472(4)	1.2475	1947.7
$Ho_{12}Pt_7In^P$	11.369(1)	14.462(2)	1.2721	1869.3
Gd_3Ga_2 [24]	11.666	15.061	1.2910	2049.7
Tb_6Al_3Si [25]	11.581	15.039	1.2986	2017.0
La_3GeIn [26]	12.308	16.078	1.3144	2435.6
$Ce_3Ge_{1.11}In_{0.89}$ [27]	12.142	15.919	1.3111	2346.9

[a] Standard deviations in the positions of the last significant digits are given in parentheses; [S]single crystal data; [P]powder data.

Table 2
Crystal data and structure refinement for $Ce_{12}Pt_7In$

Empirical formula	$Ce_{12}Pt_7In$
Molar mass (g/mol)	3161.89
Space group, Z	$I4/mcm$ (No. 140); 4
Lattice constants	$a = 12.102(2)$ Å
	$c = 14.542(3)$ Å
Calculated density (g/cm^3)	9.861
Crystal size (mm^3)	$0.30 \times 0.10 \times 0.05$
Transmission ratio (max/min)	2.11
Absorption coefficient (mm^{-1})	71.825
$F(000)$	5164
θ range for data collection	2–31°
Range in $h\,k\,l$	± 17, 17, $-11 < l < +18$
Total no. of reflections	3005
Independent reflections	842 ($R_{int} = 0.1851$)
Reflections with $I > 2\sigma(I)$	669 ($R_{sigma} = 0.1384$)
Data/restraints/parameters	842/0/33
Goodness-of-fit on F^2	1.115
Final R indices [$I > 2\sigma(I)$]	$R1 = 0.0571$; w$R2 = 0.1102$
R indices (all data)	$R1 = 0.0911$, w$R2 = 0.1219$
Extinction coefficient	0.00031(2)
Largest diff. peak and hole	6.09 and −7.37 e/Å^3

Table 3
Atomic coordinates and anisotropic displacement parameters of $Ce_{12}Pt_7In$

Atom	Site	x	y	z	Occ.	U_{eq} (Å^2)
Ce1	32(*m*)	0.0711(1)	0.2082(1)	0.14222(8)	1.00(6)	0.0050(3)
Ce2	8(*g*)	0	1/2	0.1392(1)	1.00(6)	0.0048(5)
Ce3	8(*h*)	0.1753(2)	0.6753(2)	0	1.01(6)	0.0067(5)
Pt1	16(*l*)	0.17502(7)	0.67502(7)	0.19565(7)	0.98(6)	0.0071(3)
Pt2	8(*h*)	0.6245(1)	0.1245(1)	0	1.01(6)	0.0044(4)
Pt3	4(*a*)	0	0	1/4	0.98(6)	0.0076(5)
In	4(*c*)	0	0	0	1.01(6)	0.012(1)
	U_{11}	U_{22}	U_{33}	U_{23}	U_{13}	U_{12}
Ce1	0.0037(6)	0.0040(6)	0.0072(5)	0.0024(4)	0.0000(4)	−0.0009(5)
Ce2	0.0036(9)	0.0036(9)	0.0072(9)	0	0	−0.0010(9)
Ce3	0.0066(8)	0.0066(8)	0.007(1)	0	0	0.0002(10)
Pt1	0.0075(5)	0.0075(5)	0.0062(5)	0.0005(3)	0.0005(3)	−0.0024(5)
Pt2	0.0056(6)	0.0056(6)	0.0019(6)	0	0	−0.0002(7)
Pt3	0.0012(8)	0.0012(8)	0.021(1)	0	0	0
In	0.011(2)	0.011(2)	0.015(2)	0	0	0

Note. U_{eq} is defined as one-third of the trace of the orthogonalized U_{ij} tensor.

Table 4
Interatomic distances (Å), calculated with the lattice parameters taken from X-ray powder data of $Ce_{12}Pt_7In$

Ce1:	1 Pt2	2.966(2)	*Ce2:*	2 Pt2	2.939(1)	*Pt1:*	1 Ce3	2.845(1)	
	1 Pt1	3.023(2)		2 Pt1	3.106(1)		1 Pt1	3.014(1)	
	1 Pt3	3.090(1)		1 Ce2	3.223(2)		2 Ce1	3.023(2)	
	1 Pt1	3.195(2)		2 Ce3	3.619(1)	14	1 Ce2	3.106(1)	10
	1 In	3.371(1)		4 Ce1	3.635(1)		2 Ce1	3.195(2)	
	1 Pt1	3.387(2)		2 Pt1	3.839(1)		2 Ce1	3.387(2)	
	1 Ce1	3.576(2)		1 Ce2	4.048(2)		1 Ce2	3.839(1)	
	1 Ce2	3.635(1)	15	4 Ce1	4.828(2)		1 Pt2	4.457(1)	
	1 Ce3	3.722(2)							
	2 Ce1	3.765(2)	*Ce3:*	2 Pt1	2.845(1)	*Pt2:*	2 Ce2	2.939(1)	
	1 Ce1	3.777(2)		1 Pt2	3.426(2)		4 Ce1	2.966(2)	9
	1 Ce3	3.893(2)		2 Ce2	3.619(1)		1 Ce3	3.426(2)	
	1 Ce1	3.916(2)		2 Pt2	3.680(2)	15	2 Ce3	3.680(2)	
	1 Ce1	4.136(2)		4 Ce1	3.722(2)		1 Pt2	4.262(2)	
	1 Ce2	4.828(2)		4 Ce1	3.893(2)				
				2 In	4.466(2)	*Pt3:*	8 Ce1	3.090(1)	8
In:	8 Ce1	3.371(1)	8				2 In	3.635(1)	
	2 Pt3	3.635(1)							

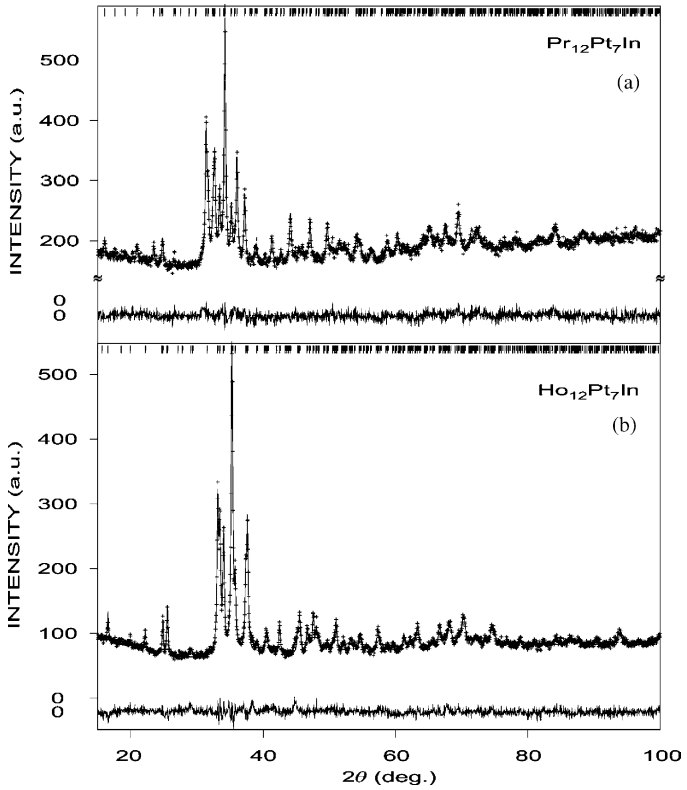

Fig. 1. Observed, calculated, and difference X-ray diffraction patterns of the $Pr_{12}Pt_7In$ (a) and $Ho_{12}Pt_7In$ (b) compounds (Cu$K\alpha$ radiation).

structure was normalized using the program Structure Tidy [26]. Listing of the observed and calculated structure factors are available.[1]

Structural refinements based on the powder intensity data collected for $Pr_{12}Pt_7In$, $Nd_{12}Pt_7In$, $Gd_{12}Pt_7In$ and $Ho_{12}Pt_7In$ revealed all these compounds to be isostructural to $Ce_{12}Pt_7In$ (Fig. 1). The atomic coordinates agree well with those for $Ce_{12}Pt_7In$ (see Tables 3 and 5). Rather high values of the residual reliability factors likely result from the complexity of the crystal structure considered. Another possible source of enhanced reliability factors can be preferred orientation of grains in powder samples studied, probably in the [001] direction.

3.2. Crystal chemistry

In Fig. 2 there are shown the crystal structure of $Ce_{12}Pt_7In$, projected on the $x-y$ plane, and the coordination polyhedra of all the atoms. This compound is the first representative of a cerium-rich (60 at%) phase formed within Ce–T–In (T-transition metal) systems that exhibits a complete atomic order in its unit cell. This is in contrast to other known structures derived from the Gd_3Ga_2-type [27], like Tb_6Al_3Si- [28] or La_3GeIn-type [29,30], where p-electron atoms are statistically distributed over the Ga sites. In the case of $Ce_{12}Pt_7In$ the 1 6 l Wyckoff positions are occupied by Pt atoms only, while all In atoms are located at the 4c sites, inside large prismatic gaps ($V_{prism} = 58.63\,Å^3$), formed by Ce1 atoms occupying the 32m positions. Smaller antiprismatic gaps ($V_{antiprism} = 44.44\,Å^3$), which also occur in Ce1 sublattice, are filled by Pt3 atoms at the 4a positions. As a result of the occupancy of the site 4a by them is the anisotropy of theirs displacement parameters. The value of U_{33} for the Pt3 atoms is high and comparable with the corresponding parameter for the In atoms because those atoms are situated practically in the channels made of tetragonal prisms and antiprisms along the [001] direction (Figs. 3a and c). But U_{11} and U_{22} are considerably smaller ($\sim$10 times) since the antiprismatic coordination sphere in comparison with prismatic one limits the oscillation of the atoms in the plane $x-y$.

Two main constituents of the $Ce_{12}Pt_7In$ structure are columns built of tetragonal antiprisms [$PtCe_8$] and prisms [$InCe_8$] (see Fig. 3a), and of clusters [$Ce_2Ce_{14}Pt_8$] (see Fig. 3b). The comparison of Gd_3Ga_2- and

[1] Further details of the crystal structure investigation can be obtained from the Fachinformationszentrum Karlruhe, 76344 Eggenstein-Leopoldshafen, Germany (fax: (49)-7247-808-666; mailto: crysdata@fiz.karlsruhe.de) on quoting the depository number CSD-413083.

Table 5
Atomic coordinates and isotropic displacement parameters of $Pr_{12}Pt_7In$ ($R_p = 2.16\%$, $R_{int} = 11.56\%$) and $Ho_{12}Pt_7In$ ($R_p = 3.66\%$, $R_{int} = 8.33\%$)

Atom	Site	x	y	z	B_{eq} (Å^2)
Pr1	32(m)	0.0728(6)	0.2047(7)	0.1420(4)	0.6(2)
Pr2	8(g)	0	1/2	0.1461(11)	0.3(4)
Pr3	8(h)	0.1747(10)	0.6747(10)	0	0.9(3)
Pt1	16(l)	0.1751(5)	0.6751(5)	0.1967(4)	1.0(2)
Pt2	8(h)	0.6252(8)	0.1252(8)	0	0.9(3)
Pt3	4(a)	0	0	1/4	1.1(4)
In	4(c)	0	0	0	1.0(7)
Ho1	32(m)	0.0715(6)	0.2062(8)	0.1427(3)	0.7(2)
Ho2	8(g)	0	1/2	0.1443(10)	1.1(4)
Ho3	8(h)	0.1737(11)	0.6737(11)	0	1.3(4)
Pt1	16(l)	0.1729(4)	0.6729(4)	0.1955(4)	0.7(1)
Pt2	8(h)	0.6215(7)	0.1215(7)	0	1.5(2)
Pt3	4(a)	0	0	1/4	0.7(4)
In	4(c)	0	0	0	1.1(6)

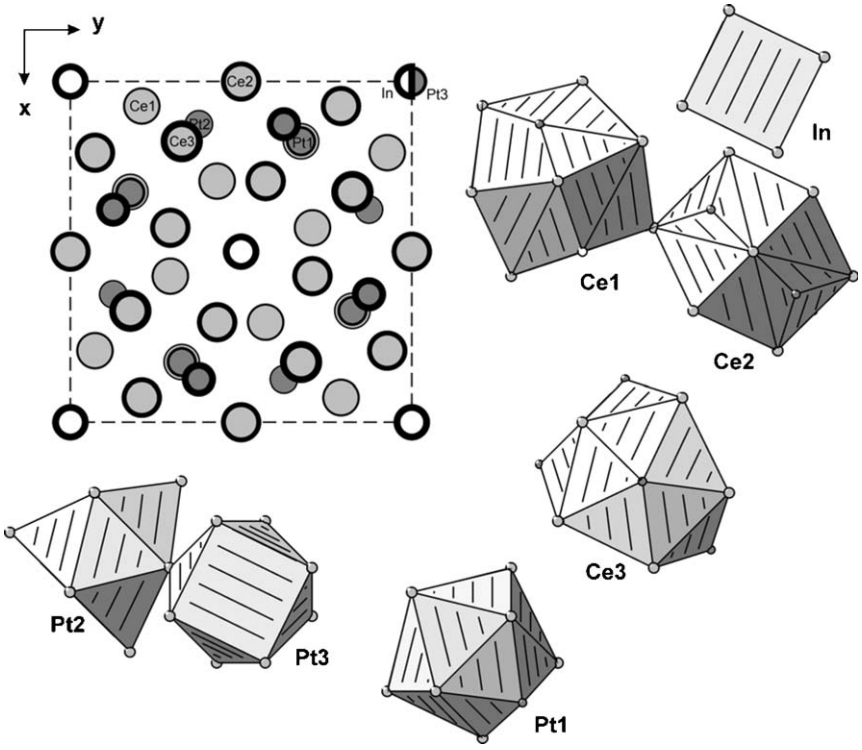

Fig. 2. Projection of the crystal structure of $Ce_{12}Pt_7In$ on the $x-y$ plane and coordination polyhedra of the atoms. Thickness of the atom's outline corresponds to their positions along the z-axis.

$Ce_{12}Pt_7In$-type structures shows that the values of δ[2] for the respective interatomic distances in the [001] direction are larger for the ternary compound (see Figs. 3c and d). In contrast, the value of δ for the atomic pairs Ce2–Ce2 inside the clusters in $Ce_{12}Pt_7In$ (11.7%) is smaller than that value which corresponds to the Gd2–Gd2 distances in the Gd_3Ga_2 structure (17.3%). Moreover, this value is also smaller than the corresponding ones in other isostructural compounds $R_{12}Pt_7In$ (14.2% for Ho2–Ho2 and Nd2–Nd2, 15.6% for Gd2–Gd2, 17.1% for Pr2–Pr2).

As a result of larger values of δ for the respective interatomic distances in the [001] direction we observe the considerably contraction of structures with Pt in the same direction. On this indicate the values of parameter c/a (see Table 1). Such behavior is characteristic of the

[2] $\delta = ((r_A + r_B - d_{AB})/(r_A + r_B))100\%$, where r_A and r_B are the atomic radii taken from Ref. [31], and d_{AB} are the respective interatomic distances.

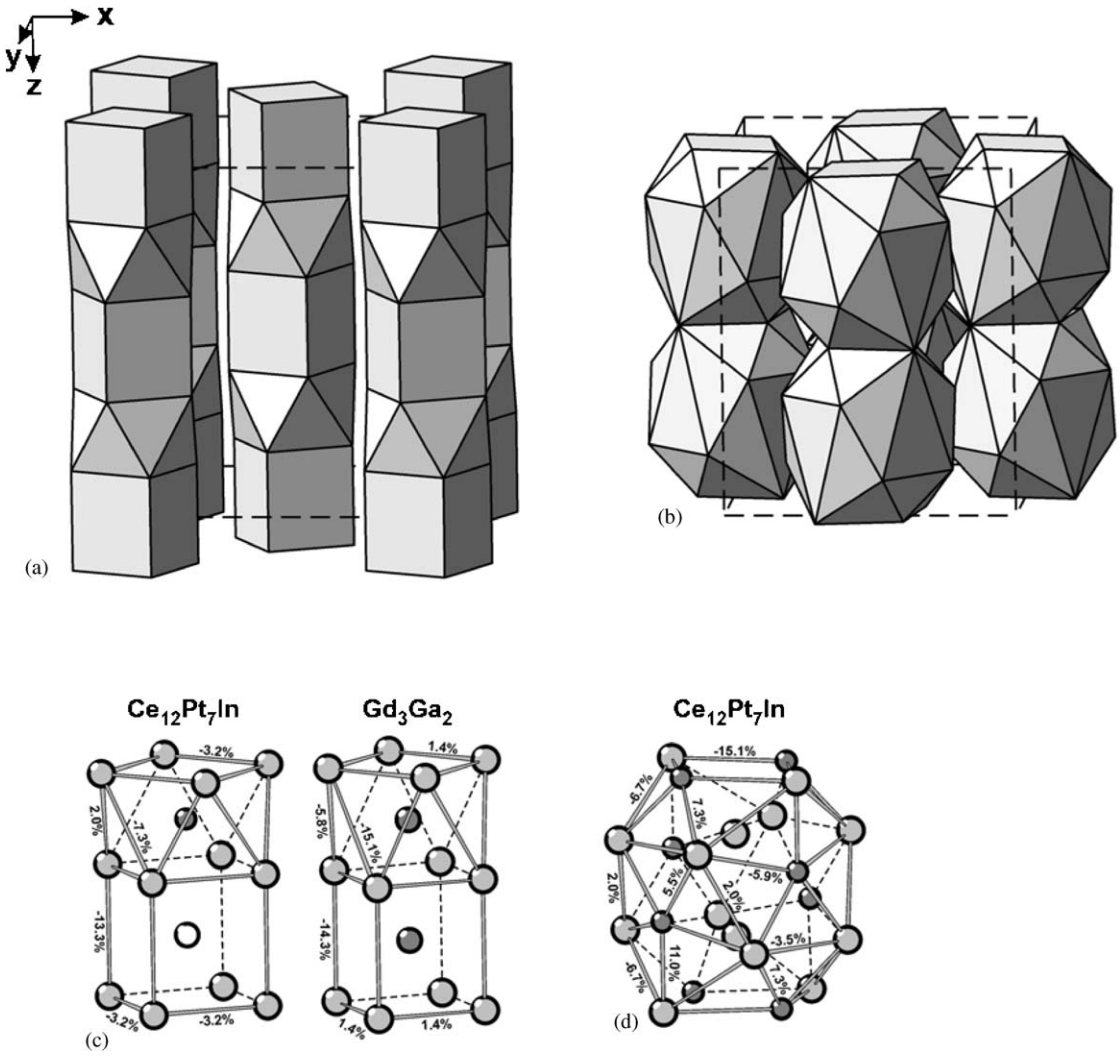

Fig. 3. Three-dimensional arrangement of columns consisting of tetragonal antiprisms [$PtCe_8$] and tetragonal prisms [$InCe_8$] (a), and clusters [$Ce_2Ce_{14}Pt_8$] (b), characteristic of the $Ce_{12}Pt_7In$ structure. Detailed view of fragments of the columns (c) and clusters (d) for both $Ce_{12}Pt_7In$- and Gd_3Ga_2-type structures. The values of δ for some main bonds are given. The cerium (gadolinium), platinum (gallium), and indium atoms are drawn as light gray, dark gray and open circles, respectively.

compounds $R_xT_yIn_z$ with high content of rare earths. Analogous compounds $R_xT_yAl_z$ or $R_xT_yGa_z$ have mainly larger values of parameter c/a [32]. On the other hand, the considerably contraction of novel structures can be explained by the role of the Pt atoms (most electronegative comparing with other atoms). Gd_3Ga_2 is a multilayer structure along the direction [001] and four layers consist exceptionally of the atoms of rare earths. The change of the Ga atoms on the more electronegative Pt ones enhances mainly the interaction between layers and less inside of layers, what leads to the increase of parameter c/a.

Inspecting the change in the values of the lattice parameters in the $R_{12}Pt_7In$ series one notices that c initially changes from Ce to Pr and after that is almost independent of the R component. However, parameters a and V strongly decreases with decreasing the radius of R^{+3} ion [33] according to lanthanoid contraction (see Fig. 4).

3.3. Magnetic and electrical properties of $R_{12}Pt_7In$

Fig. 5 presents the inverse magnetic susceptibility of (a) $Ce_{12}Pt_7In$, (b) $Pr_{12}Pt_7In$ and (c) $Nd_{12}Pt_7In$ as a function of the temperature. In the case of Ce- and Nd-based compounds the $\chi^{-1}(T)$ curves exhibit a linear behavior above about 100 K and can be well described by the Curie–Weiss law (see the solid lines in Figs. 5a and c) with the effective magnetic moments $\mu_{eff} = 2.45\,\mu_B$ and $3.75\,\mu_B$, and the paramagnetic Curie temperatures $\theta_p = -23.5$ and 5.75 K, respectively. In contrast, $\chi^{-1}(T)$ measured for $Pr_{12}Pt_7In$ is strongly curvilinear in the whole temperature range studied. Above 80 K the experimental data follow the modified

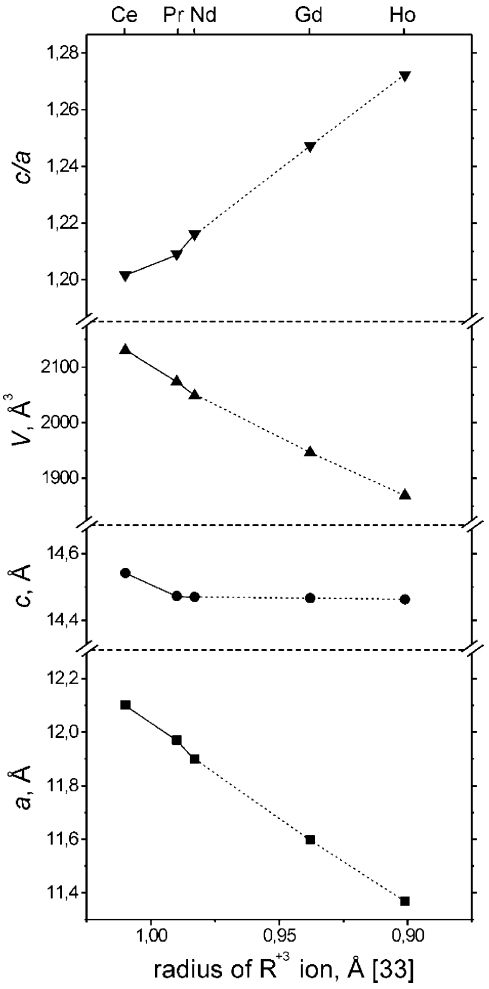

Fig. 4. Dependence of the lattice parameters of $R_{12}Pt_7In$ compounds vs. the radii of respective R^{+3} ions [31].

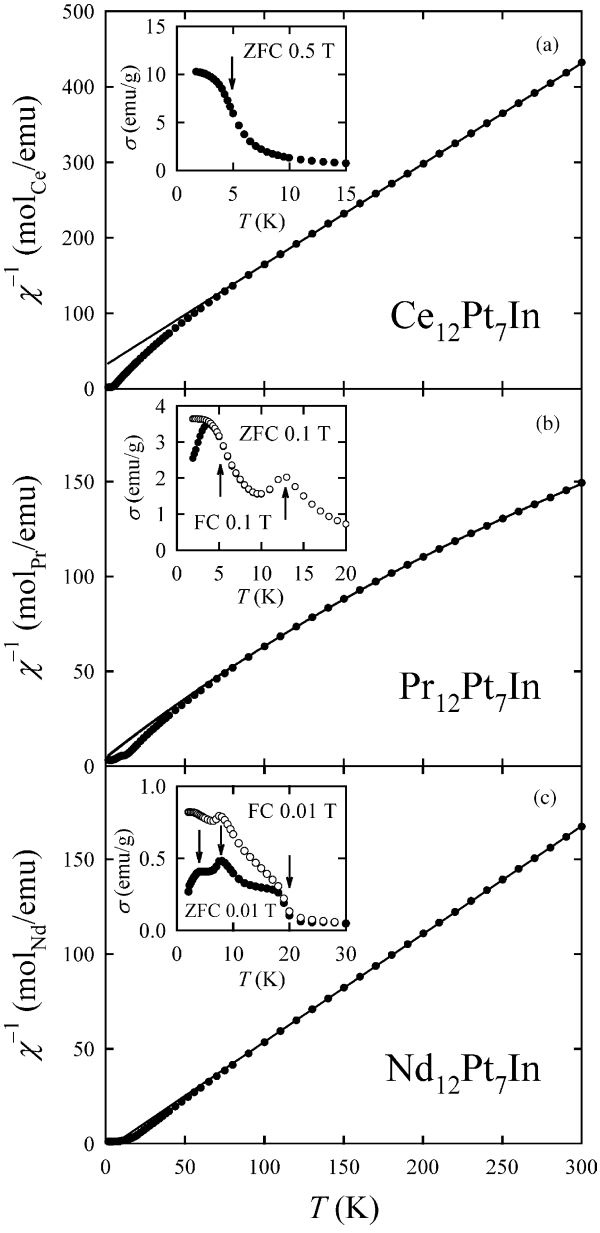

Fig. 5. Temperature dependencies of the inverse magnetic susceptibility of $R_{12}Pt_7In$ compounds, measured in a field of 0.5 T ($Ce_{12}Pt_7In$) or 0.1 T ($Pr_{12}Pt_7In$ and $Nd_{12}Pt_7In$). The solid lines are the Curie–Weiss fits to the experimental data. The insets display the magnetization as a function of temperature measured in zero-field cooling (ZFC, closed circles) and field cooling (FC, open circle) regimes. The arrows mark the magnetic phase transitions.

Curie–Weiss law $\chi(T) = C/(T-\theta_p) + \chi_0$, where χ_0 represents Pauli-like paramagnetic susceptibility. The least-squares fitting procedure (see the solid line in Fig. 5b) yields the following parameters: $\mu_{eff} = 3.45\,\mu_B$, $\theta_p = -6.8\,K$ and $\chi_0 = 18.5 \times 10^{-4}\,emu/mol_{Pr}$. It is worthwhile noting that the experimental values of μ_{eff} are rather close to those expected for free Ce^{3+}, Pr^{3+} and Nd^{3+} ions ($\mu_{eff} = g\sqrt{j(j+1)} = 2.54$, 3.58 and $3.62\,\mu_B$, respectively).

At low temperatures all three compounds studied exhibit transitions to magnetically ordered state. As may be inferred from the insets to Fig. 5, the character of magnetic ordering in these materials is rather complex. Assuming that the samples studied were single phase such a behavior may be attributed to the presence in the structure of as many as three positions of the rare-earth atoms, each defining its own magnetic sublattices. For $Ce_{12}Pt_7In$ a ferromagnetic-like temperature dependence of the magnetization is observed below ca. 5 K. $Pr_{12}Pt_7In$ orders antiferromagnetically at ca. 13 K but shows another phase transition at about 5 K, possibly to canted antiferromagnetic or ferrimagnetic state, as presumed from a characteristic irreversibility seen in the magnetization taken in zero-field-cooled (ZFC) and field-cooled (FC) conditions. In turn, $\sigma(T)$ of $Nd_{12}Pt_7In$ is ferromagnetic-like below about 20 K, but exhibits quite complicated behavior at lower temperatures, which suggests complex character of the magnetic ordering with possible spin reorientation around 9 K.

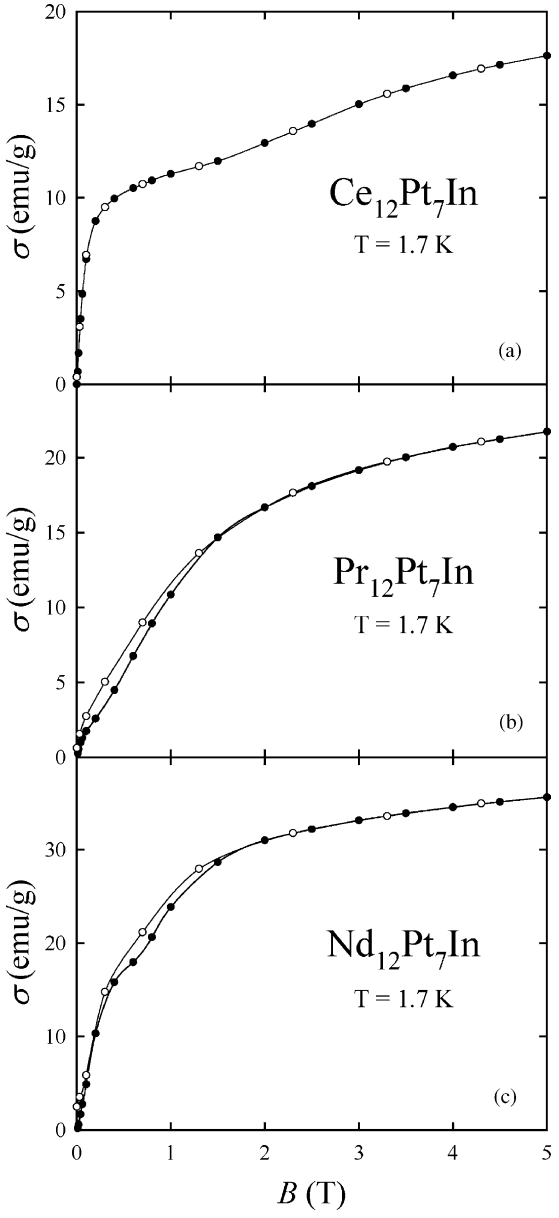

Fig. 6. Magnetization of $R_{12}Pt_7In$ compounds as a function of magnetic field taken at $T = 1.7$ K with increasing (closed circles) and decreasing (open circles) field. The solid lines serve as a guide for the eye.

The presence of ferromagnetic components in the magnetic structures of the $R_{12}Pt_7In$ compounds studied as well as the complexity of their overall character are corroborated by the field variations of the magnetization measured at 1.7 K. The $\sigma(B)$ curves presented in Fig. 6 show a two-step saturation behavior that may be attributed to spin rearrangements induced by magnetic field. The magnetic moments reached at 5 T amount to 0.85, 1.0 and 1.68 μ_B for $Ce_{12}Pt_7In$, $Pr_{12}Pt_7In$ and $Nd_{12}Pt_7In$, respectively, being in all cases much smaller than the values calculated for free ions ($\mu_{ord} = gj = 2.14$, 3.2 and 3.27 μ_B, for Ce^{3+}, Pr^{3+} and Nd^{3+}, respectively).

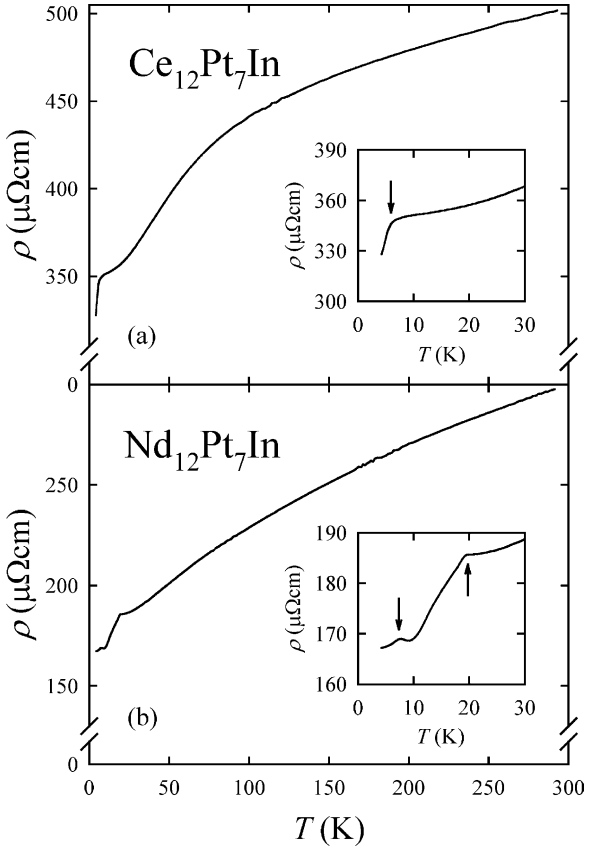

Fig. 7. Electrical resistivity of $Ce_{12}Pt_7In$ and $Nd_{12}Pt_7In$ vs. temperature. The insets show the low temperature resistivity. The arrows mark the magnetic phase transitions.

This reduction may be largely attributed to crystal field effects, but also to the complexity of the magnetic structures of the compounds considered.

Fig. 7 presents the temperature dependence of the resistivity of $Ce_{12}Pt_7In$ and $Nd_{12}Pt_7In$. In the paramagnetic region $\rho(T)$ of the cerium compound shows features characteristic of Kondo systems with strong crystal–field interactions. The resistivity is rather large (ca. 500 μΩ cm at 300 K) and exhibits a hump around 100 K due to thermal population of crystal field levels. The magnetic ordering at 5 K manifests itself as a salient kink in $\rho(T)$. A similar anomaly is observed for $Nd_{12}Pt_7In$ at 20 K, i.e., at the temperature of ferromagnetic phase transition. In addition, for this compound there is visible a small peak in $\rho(T)$ at 8 K that may be associated with another magnetic phase transition observed at this temperature in $\sigma(T)$ (compare Fig. 5c).

Acknowledgments

The authors are grateful to Mr. K. Nierzewski for EDAX measurements. This work was partially

supported by the State Committee of Scientific Research KBN (Grant No. 2 P03B 028 23).

References

[1] R. Ferro, R. Marazza, G. Rambaldi, Z. Anorg, Allg. Chem. 410 (1974) 219.
[2] H. Hulliger, J. Alloys Compds. 217 (1995) 164.
[3] Ya.V. Galadzhun, R. Pöttgen, Z. Anorg, Allg. Chem. 625 (1999) 481.
[4] V. Zaremba, Ya. Galadzhun, Ya. Kalychak, D. Kaczorowski, J. Stępień-Damm, J. Alloys Compds. 296 (2000) 280.
[5] Ya.V. Galadzhun, V.I. Zaremba, H. Piotrowski, P. Mayer, R.-D. Hoffmann, R. Pöttgen, Z. Naturforsch 55B (2000) 1025.
[6] V.I. Zaremba, Y.V. Galadzhun, B.D. Belan, A. Pikul, J. Stępień-Damm, D. Kaczorowski, J. Alloys Compds. 316 (2001) 64.
[7] U.Ch. Rodewald, V.I. Zaremba, Ya.V. Galadzhun, R.-D. Hoffmann, R. Pöttgen, Z. Anorg. Allg. Chem. 628 (2002) 2293.
[8] V.I. Zaremba, Ya.M. Kalychak, V.P. Dubenskiy, R.-D. Hoffmann, U.Ch. Rodewald, R. Pöttgen, J. Solid State Chem. 169 (2002) 118.
[9] S.K. Malik, R. Vijayaraghavan, D.T. Adroja, B.D. Padalia, A.S. Edelstein, J. Magn. Magn. Mater. 92 (1990) 80.
[10] D. Rossi, D. Mazzone, R. Marazza, R. Ferro, Z. Anorg. Allg. Chem. 507 (1983) 235.
[11] H. Fujii, Y. Uwatoko, M. Akayama, K. Satoh, Y. Maeno, T. Fujita, J. Sakurai, H. Kamimura, T. Okamoto, Jpn. J. Appl. Phys. Suppl. 26 (3) (1987) 549.
[12] T. Fujita, K. Satoh, Y. Maeno, Y. Uwatoko, H. Fujii, J. Magn. Magn. Mater. 76–77 (1988) 133.
[13] Y. Yamaguchi, J. Sakurai, F. Teshima, H. Kawanaka, T. Takabatake, H. Fujii, J. Phys.: Condens. Matter 2 (1990) 5715.
[14] M. Kurisu, T. Takabatake, H. Fujii, J. Magn. Magn. Mater. 90–91 (1990) 469.
[15] K. Satoh, T. Fujita, Y. Maeno, Y. Uwatoko, H. Fujii, J. Phys. Soc. Jpn. 59 (1990) 692.
[16] H. Fujii, T. Takabatake, Y. Andoh, J. Alloys Compds. 181 (1992) 111.
[17] D. Kaczorowski, P. Rogl, K. Hiebl, Phys. Rev. B. 54 (1996) 9891.
[18] R. Hauser, H. Michor, E. Bauer, G. Hilscher, D. Kaczorowski, Physica B 230–232 (1997) 211.
[19] M.F. Hundley, J.L. Sarrao, J.D. Thompson, R. Movshovich, M. Jaime, Phys. Rev. B. 65 (2001) 024401.
[20] V.I. Zaremba, Ya.V. Galadzhun, Ya.M. Kalychak, V.M. Davydov, J. Stępień-Damm, A. Pietraszko, Proceedings of Seventh International Conference on Crystal Chemistry of Intermetallic Compounds, Lviv, Ukraine, 1999, p. B24.
[21] J.M. Kalychak, V.I. Zaremba, P.Y. Zavalij, Z. Kristallogr. 208 (1993) 380.
[22] Ya.M. Kalychak, V.I. Zaremba, J. Stępień-Damm, Ya.V. Galadzhun, L.G. Akselrud, Kristallografia (in Russian) 43 (1998) 17.
[23] DBWS-9807—upgrade of: "DBWS-9411—an upgrade of the DBWS programs for Rietveld Refinement with PC and mainframe computers", J. Appl. Cryst. 28 (1995) 366.
[24] G.M. Sheldrick, SHELXS-97, Program for the Solution of Crystal Structures, University of Göttingen, Germany, 1997.
[25] G.M. Sheldrick, SHELXL-97, Program for the Crystal Structure Refinement, University of Göttingen, Germany, 1997.
[26] E. Parté, K. Cenzual, R. Gladyshevskii, J. Alloys Compds. 197 (1993) 291.
[27] S.P. Yatsenko, R.E. Hladyschewsky, O.M. Sitschewitsch, V.K. Belsky, A.A. Semyannikov, Yu.N. Hryn, Ya.P. Yarmolyuk, J. Less-Comm. Metals 115 (1986) 17.
[28] I.S. Dubenko, A.A. Evdokimov, V.M. Ionov, Kristallografia (in Russian) 32 (1987) 347.
[29] A.M. Guloy, J.D. Corbett, Inorg. Chem. 35 (1996) 2616.
[30] G. Nychyporuk, V. Zaremba, Ya. Kalychak, J. Stępień-Damm, A. Pietraszko, J. Alloys Compds. 312 (2000) 154.
[31] E. Teatum, K. Gschneidner, J. Waber, Los Alamos Scientific Laboratory Report LA-2345, US Department of Commerce, Washington, DC, 1960.
[32] Ya.M. Kalychak, Proceedings of Eighth International Conference on Crystal Chemistry of Intermetallic Compounds, Lviv, Ukraine, 2002, p. L2.
[33] R.D. Shannon, Acta Crystallogr. A 32 (1976) 751.